Supplemental Information

Controllable Generation of Reactive Oxygen Species

on Cyano-Group-Modified Carbon Nitride for Selective

Epoxidation of Styrene

Hao Tan, Peng Kong, Riguang Zhang, Mengting Gao, Meixian Liu, Xianmo Gu, Weifeng Liu, and Zhanfeng Zheng

Supplemental Note: Case Reports

1. Supplemental Methods.

1.1 Bulk *CN*. Melamine (10 g) was heated in a crucible using a muffle furnace at 550 °C for 4 h, with a ramp rate of 3 K/min under ambient atmosphere. The light-yellow product was ground thoroughly prior to characterization.

1.2 *CND, CN$_{th}$, CNDT and CNMT*. The synthetic method for CND and CN$_{th}$ is similar to the above bulk CN, except using dicyandiamide and thiourea as precursor, respectively. CNDT and CNMT sample was prepared by mixing 0.3 g of thiourea with 10 g of dicyandiamide and melamine respectively and then heated in a crucible using a muffle furnace at 550 °C for 4 h, with a ramp rate of 3 K/min under ambient atmosphere.

1.3 *CN (KSCN)* in Table 1, entry 3. The synthetic method for CN is identical to the above bulk CN. KSCN treated CN was synthesized by thoroughly grounding CN (800 mg) with KSCN (1.6 g, dried at 140 °C in vacuum) and loaded in an alumina boat. In a tube furnace, this mixture was heated under argon to 400 °C at 30 °C/min ramp for 1 h, and then to 500 °C at 30 °C/min ramp for 30 min. The resulting yellow mass was suspended in water and the insoluble product was isolated by centrifugation, washed with copious amount of water and dried at 60 °C in a vacuum oven.[1]

1.4 *CN and CNQ680* in Table 1, entries 4 and 5. Pristine graphitic carbon nitride was synthesized using thermal polymerization of dicyandiamide (Aldrich, 99%) at 480 °C for 4 h, with the ramping rate of 2 °C/min in a muffle furnace in air. The resultant yellow agglomerates were milled into powder in a mortar (the sample was named as CN). For the quick thermal treatment, a horizontal tube furnace was heated to target temperatures 680 °C and 250 mg of

g–C_3N_4 was put in an alumina crucible. A stopwatch was started as soon as the alumina crucible was placed at the targeted heating zone. When the watch ran for 5 min, the crucible was fished out as soon as possible and cool down in air. The whole process is carried out in well ventilated space. The resulting products were collected and named as CNQ680.[2]

1.5 Bulk g–C_3N_4 and ribbon–like g–C_3N_4 in Table 1, entries 6 and 7. As a typical procedure, dicyandiamide and NaCl with the mass ratio of 1:1 were mixed and ground to fine powders using a mortar and pestle. Then in nitrogen atmosphere, the fine powders were heated from room temperature to 600 °C at a rate of 19.3 °C/min and kept at 600 °C for 60 min. After cooling to room temperature, 1 g obtained orange sample was grounded, added into 100 mL deionized water and sonicated for 30 min. The dispersion was centrifuged at 4000 rpm for 10 min to obtain a homogenous dispersion. Then the dispersion was freeze–dried, and the target sample was finally obtained. The bulk g–C_3N_4 was prepared as a reference by heating dicyandiamide using the same heating procedure.[3]

1.6 g–C_3N_4 and g–C_3N_4–0.01 in Table 1, entries 8 and 9. Pristine g–C_3N_4 was prepared by urea pyrolysis according to a standard literature method. Briefly, 15 g of urea was calcined at 450 °C in a muffle furnace for 1 h using a heating rate of 10 °C/min. g–C_3N_4–0.01 was synthesized as follows: 15 g of urea was dissolved with stirring into aqueous KOH solutions (KOH 0.01 g in 30 mL H_2O), and then the resulting solution evaporated to dryness in an oven at 80 °C overnight. The solid mixtures of urea and KOH were then calcined at 450 °C in a muffle furnace for 4 h using a heating rate of 10 °C/min. Products were denoted as g–C_3N_4–0.01. Following synthesis, all samples were washed with water to remove any residual alkali.[4]

1.7 *CN and DCN–200* in Table 1, entries 10 and 11. The pristine g–C_3N_4 was prepared by the commonly used direct thermal polymerization of dicyandiamide at 550 °C for 4 h with a ramping rate of 3 °C/min in air. After cooled naturally, the yellow product was grounded in an agate mortar to obtain a powder sample. To prepare the defect–modified homojunction g–C_3N_4, the pristine g–C_3N_4 was fully mixed with $NaBH_4$ with a weight ratio of 5:1, followed by heating at 200 °C for 30 min. Then the resultant powders were washed with water, HCl, NaOH, and once again with water (washed several times until neutral) to remove all unreacted and potentially detrimental surface species. The products were denoted as DCN–200 °C.[5]

1.8 Cyano hydrolysis method. In typical procedure, 600 mg of the $CNCY_x$ was dispersed in 200 mL of sulphuric acid solution (3 M) and reflux in 80 °C for 2 h, this sample was named as $CNCY_x$–H. The resulting yellow mass was suspended in water and the insoluble product was isolated by centrifugation, washed with copious amount of water until the filtrate is neutral and dried at 60 °C in a vacuum oven.

2. Supplemental In situ Diffuse Reflectance Infrared Experiments.

The setup was consisted of the following parts: (i) a Bruker Tensor II FT-IR spectrometer equipped with a MCT detector; (ii) a Praying Mantis™ HVC accessory enclosed with a three-window dome; (iii) a HARRICK ATC-024-4 temperature controller; (iv) a cooling water circulating system; (v) a xenon lamp. Highly purity Ar (25 mL·min⁻¹) was used as the carrier gas (Figure S2a).

The tests were carried out according to the following procedures. (1) The fresh powder sample was loaded in the *in situ* reaction cell (Figure S2b). (2) After assembling the HVC with a sample into the spectrometer, the system was warmed to 120 °C with the inlet of Ar gas (25

mL·min^{-1}) for 3 h. The temperature was controlled by the ATC controller and cooling water. (3) After the thermal treatment, until the HVC was cooled to 30 °C, 20 μL of the styrene was introduced to the HVC by dripping. (5) The cell was purged by the Ar gas (25 mL·min^{-1}) to clean up the redundant substrates, until the IR signals stable. (6) The outlet of the cell was sealed and additional 5 mL oxygen was injected into the cell through the latex tube which connected with the intake of the cell (Figure S2c). (7) Samples were irradiated by means of a solar light simulator with a xenon lamp. The solar light simulator was equipped with a cut 420 nm filter to remove ultraviolet irradiation. Meanwhile, IR spectra were collected repeatedly every 1 min (Figure S2c).

3. Supplemental Photoactivity Measurements.

The styrene epoxidation reactions were conducted under air atmosphere (1 atm) in a 25 mL round-bottomed Pyrex glass flask with a sealed spigot and a magnetic stirrer (Figure S9). The suspensions were prepared by mixing styrene (0.04 mmol), acetonitrile (2 mL), and catalyst (10 mg) in a reactor equipped with a stirrer bar. The reactor was irradiated using a white LED light (400 mW/cm^2) whilst stirring at 60 °C. The product compositions were analyzed and determined by means of an Agilent HP5973 mass spectrometer and Agilent 1260 high efficiency liquid chromatography. The Agilent Series are equipped with a vacuum degasser, a quaternary pump, an auto sampler and a DAD system, connected to Agilent Chem Station software. A C18 column (250×4.6 mm i.d., 5 μm) was used. The flow rate was 1 mL/min. Solvents that constituted the mobile phase were (A) acetonitrile and (B) water with the volume ratio 65:35. The products were also identified by mass spectrometry (GC-MS, Agilent 6890N) coupled with 5973 Mass selective Detector.

4. Supplemental Quantification methods.

The conversion of styrene and the selectivity of styrene oxide, and benzaldehyde were analysed by HPLC by using the external standard method.

5. Supplemental Acidimetric titration of carbon nitride.

The acidic functional groups and the presences of such groups were determined by a neutralization adsorption experiment. Typically, 100 mg (m_1) $CNCY_{1.00}$ and CNCY–H sample were dispersed into 50 g (m_A) of 0.05 mol/L $NaHCO_3$ aqueous solution, respectively. The resultant mixtures were allowed to equilibrate with magnetic stirring for 6 h. After that, the mixtures were filtered and the filtrate was collected and 20 g (m_{A1}) of the filtrate or 20 g $NaHCO_3$ aqueous solution (m_{A0}) was pipetted out and back titrated using 0.025 mol/L (C) hydrochloric acid solutions. Recording the volume of hydrochloric acid consumed as V_{A1} and V_{A0}. The concentrations of the $NaHCO_3$ aqueous solution were calibrated by standard hydrochloric acid. In the controlled reaction 50 g (m_F) water was used to disperse 100 mg (m_2) of the sample. After stirring for 6 h, 10 g filtrate (m_{F1}) was mixed with 25 g NaOH (m_{FC}) aqueous solution (FC mixture) and back titrated using 0.025 mol/L hydrochloric acid solutions to determination of the acidity and alkalinity of the catalyst surface. Recording the volume of hydrochloric acid consumed as V_F. Bromocresol green–methyl red was used as the indicator. The adsorbed base was calculated using the following equation:

$$n_A = \left(V_{A0} * \frac{C}{m_{A0}} - V_{A1} * \frac{C}{m_{A1}}\right) * \frac{m_A}{m_1} + n_F \qquad \text{(s1)}$$

$$n_F = \left[\left(V_F * C - V_{C0} * \frac{C*m_{FC}}{m_{C0}}\right)/m_{F1}\right] * m_F/m_2 \qquad \text{(s2)}$$

In the equations:

  C : Concentration of standard hydrochloric acid (mol/L);

V_{A0}: The hydrochloric acid volume used in calibrating base solution (mL);

m_{A0}: The quality of base solution used in calibrating by hydrochloric acid (g);

V_{A1}: The hydrochloric acid volume used in calibrating the above filtrate (mL);

m_{A1}: The quality of base filtrate solution used in titration (g);

m_A: The quality of base solution used in sample dispersion (g);

m_1, m_2: The consumption quality of our sample (g).

V_F: The hydrochloric acid volume used in calibrating FC mixture (mL);

m_{FC}: The quality of FC mixture used in titration (g);

m_{F1}: 10 g;

m_F: The quality of water used in sample dispersion (g).

6. Supplemental Quantitative determination of hydrogen peroxide content by iodometry.

The H_2O_2 generated in the reaction were determined by a typical iodometry method. Typically, 2 mL of reaction solution was filtered after illumination for 6 h, then 10 μL of sulfuric acid solution (1 mL sulphuric acid mixed with 8 mL deionized water) was dropped into the above filtrate. After that, 1 g of KI and 30 μL of ammonium molybdate (30 g/L) were added in turn, the resultant mixtures were allowed to equilibrate with magnetic stirring for 5 minutes. Finally, the mixtures were titrated using $Na_2S_2O_3$ and Na_2CO_3 mixture solution (25 g/L of $Na_2S_2O_3 \cdot 5H_2O$, 0.2 g/L of Na_2CO_3) until the solution becomes colourless. In the controlled reaction water was used to as the contrast. The reactions between H_2O_2, I_2 and $Na_2S_2O_3$ were showed as below.

$$H_2O_2 + 2I^- + 2H^+ = 2H_2O + I_2 \qquad (s3)$$

$$I_2 + 2Na_2S_2O_3 = 2NaI + Na_2S_4O_6 \qquad (s4)$$
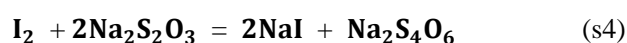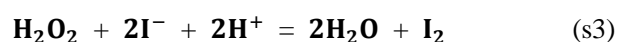
According to the reaction equation the H_2O_2 content is equal with two stoichiometric ratios of

$Na_2S_2O_3$.

7. Supplemental Photoelectrochemical (PEC) Measurements.

The working electrode was prepared by the drop-casting method. In a typical process, 5 mg of the catalyst powder was mixed with 0.5 g of 2 wt.% polyvinylidene difluoride (PVDF) N–methyl pyrrolidone (NMP) solution by sonication, then 20 μL of the slurry was dropped onto fluorine-doped tin oxide (FTO, 2 cm × 1.5 cm) glass electrode through a layer-by-layer method. Photocurrent measurements were performed under LED light illumination conditions in a 0.2 M Na_2SO_4 solution by using the Amperometric it Curve technique with the pH maintained at 6.6. Mott–Schottky plots were also obtained with the working electrodes immersed in 0.2 M Na_2SO_4 aqueous solution, yet, by using the impedance–potential technique. The potential conversion relation is according to the Nernst equation:

$$E(NHE) = E(Ag/AgCl) + 0.197 \qquad (s5)$$

$$E(RHE) = E(NHE) + 0.0591 \times pH \qquad (s6)$$

Note: The potential of RHE is related to pH value, when the pH = 0, the potential of RHE is equivalent to SHE.

The electrochemical impedance spectra (EIS) were obtained by using the A. C. Impedance technique. The working electrodes were immersed in mixture aqueous solution. The composition of the mixture solution was as follows: 0.1 mol/L KCl, 2 mmol/L $K_3[Fe(CN)_6]$ and 2 mmol/L $K_4Fe(CN)_6 \cdot 3H_2O$. All the above tests were characterized on a workstation (CHI 760D, CH Instruments, Inc., Shanghai, China) in a three–electrode model, with Pt wire as the counter electrode and Ag/AgCl electrode (saturated KCl) as the reference electrode.

8. Supplemental Computational Methods.

All density functional theory calculations (DFT) calculations were implemented in Dmol^3 program package of Materials Studio 8.0.[6, 7] The exchange-correlation functional PBE was used to calculate the electronic structure with generalized gradient approximation (GGA).[8, 9] The valence electron functions were expanded into a set of numerical atomic orbital by a double numerical basis with polarization functions (DNP).[10, 11] All atoms were treated with an all-electron basis set. Meth fessel–Paxton smearing of 0.005 Ha was adopted. The dispersion-corrected (DFT-D2) method is used to describe the dispersion interaction. All energies obtained in our calculations included the zero-point vibrational energy
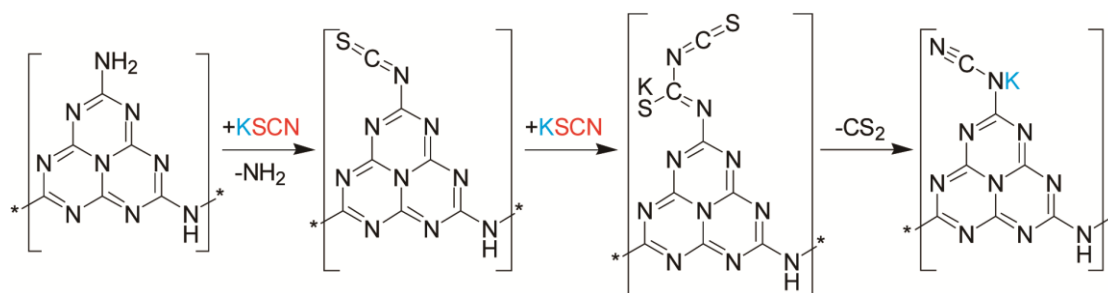
Scheme S1. Proposed cyano introduction mechanism by KSCN assisted synthesis.
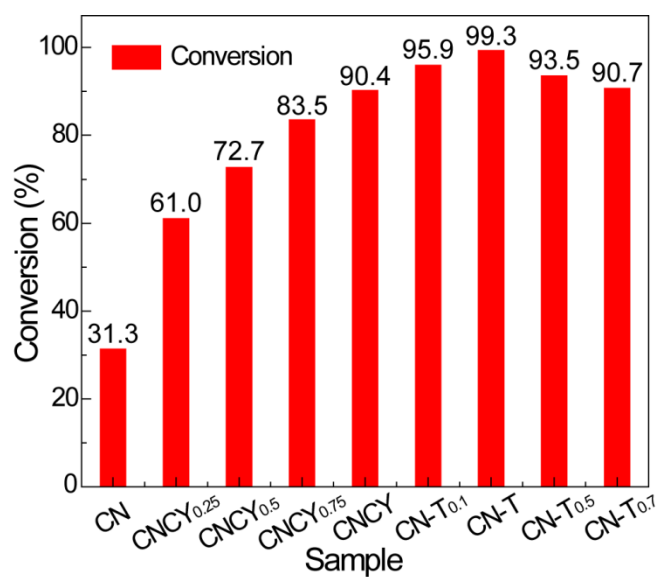
Figure S1. Styrene conversion rate as the function of cyano group content in carbon nitride.

Reaction condition: 0.04 mmol of the styrene, 2 mL of the acetonitrile, 10 μL of the isobutyraldehyde, 15 mg of the catalyst, 1 atm Air, 400 mW/cm^2 irradiation, white LED light, 60 °C, 2 h.

The isobutyraldehyde was used as the reduction reagent, the selectivity for styrene oxide by using CN and CN-T is 45% and 87%, respectively. Thus, the yield of styrene oxide by using CN and CN-T is 14.1% and 86.4%, respectively.
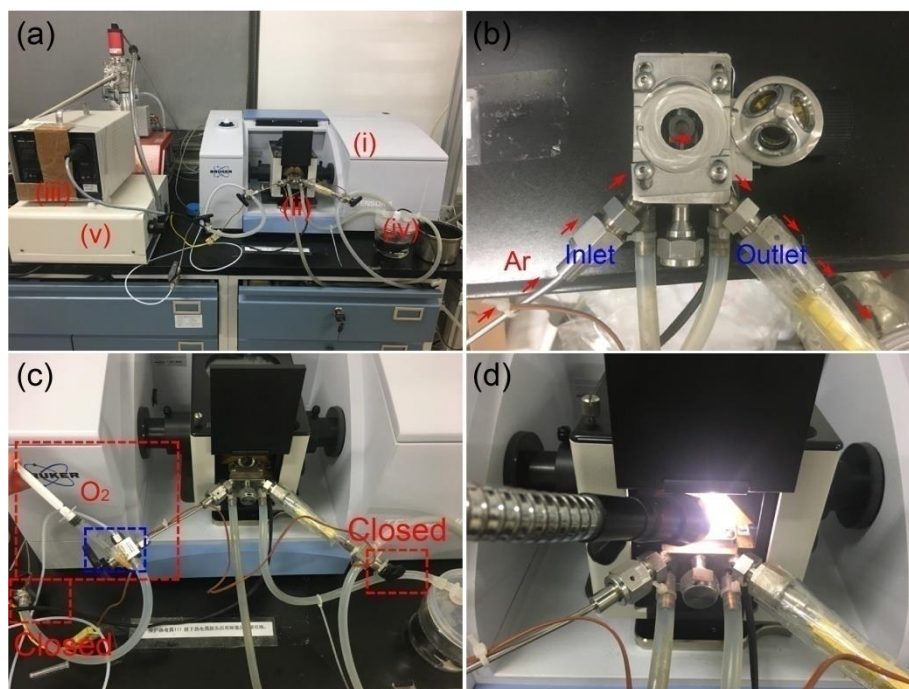
Figure S2. Photographs of (a) *in-situ* FT-IR setup. (b) HVC accessory enclosed with a three-window dome. (c) Oxygen injection methods. (d) Light illumination.

In Figure S2, the digital coding represents (i) Bruker Tensor Ⅱ FTIR spectrometer, (ii) HVC accessory, (iii) HARRICK ATC-024-4 temperature controller, (iv) cooling water circulating system and (v) Xenon lamp. Before the oxygen injection, the two three-way valves (red box) in Figure S2c were closed. The oxygen (5 mL) was injected by using 2.5 mL needle tube, after that the three-way valve in the blue box was closed until the end of the test.
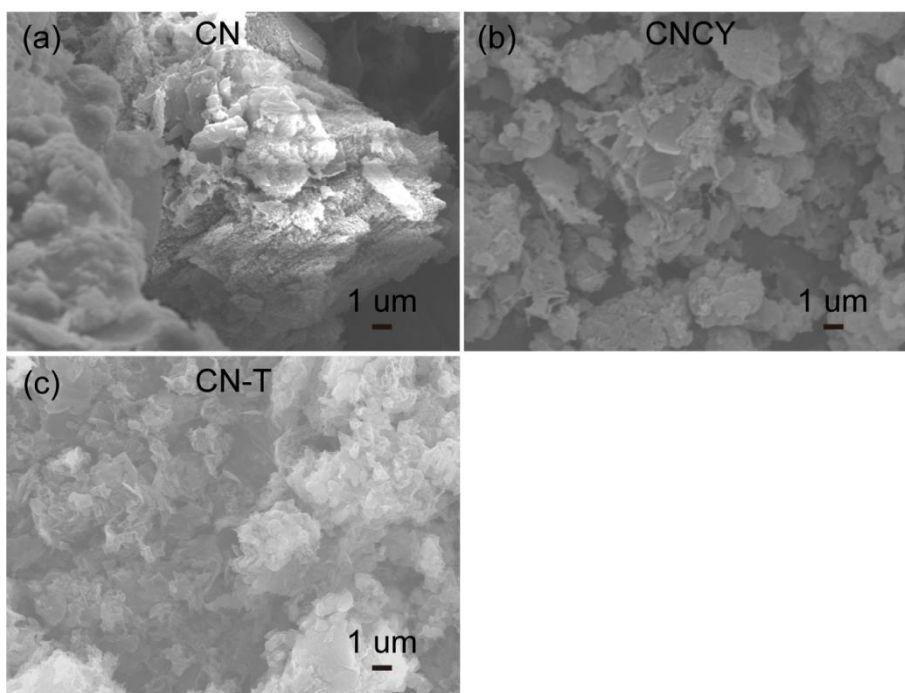
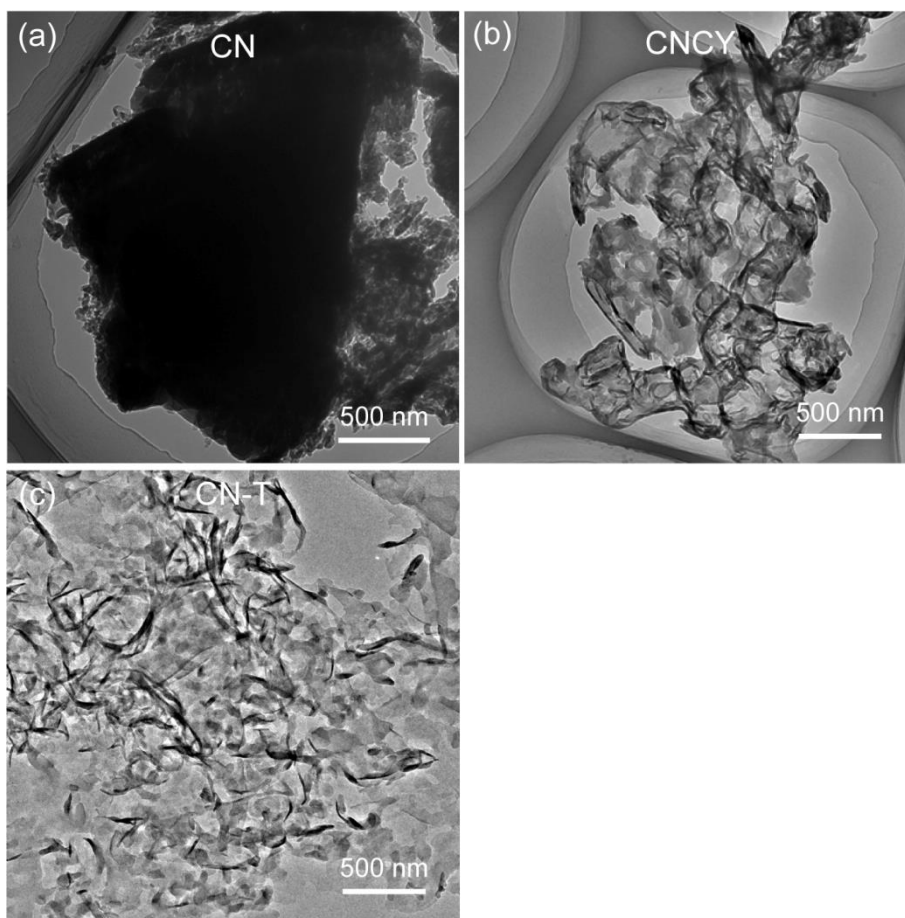**Figure S3.** The SEM spectra of sample (a) CN, (b) CNCY and (c) CN-T.

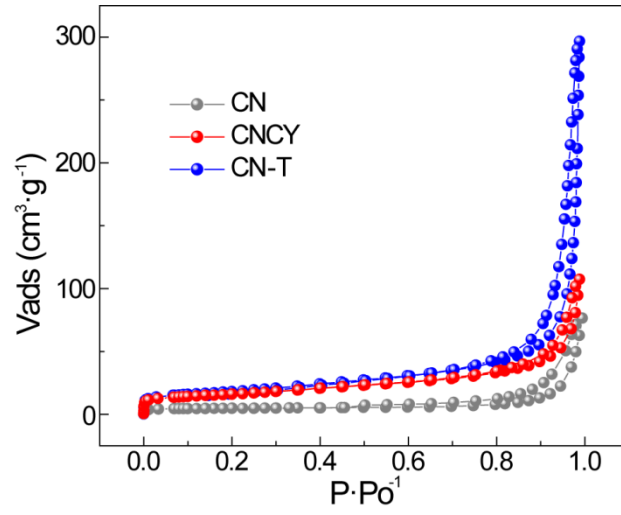**Figure S4.** The TEM spectra of sample (a) CN, (b) CNCY and (c) CN-T.

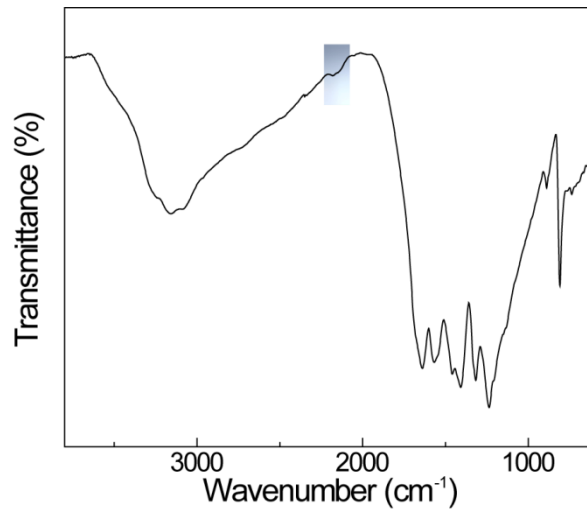**Figure S5.** Adsorption isotherms spectra of CN, CNCY and CN-T.
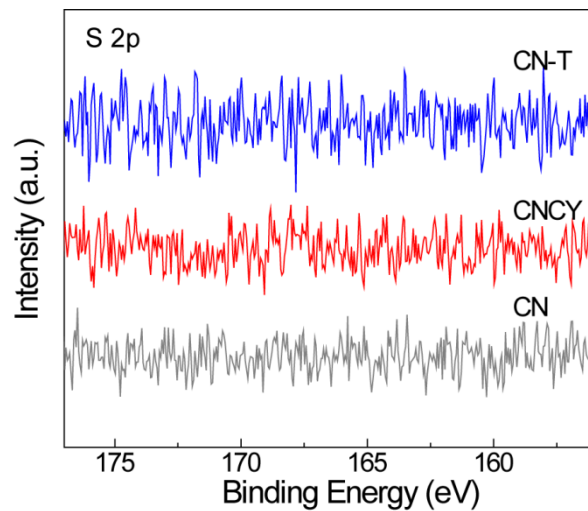

Figure S6. The FT–IR spectra of CN_{th}.
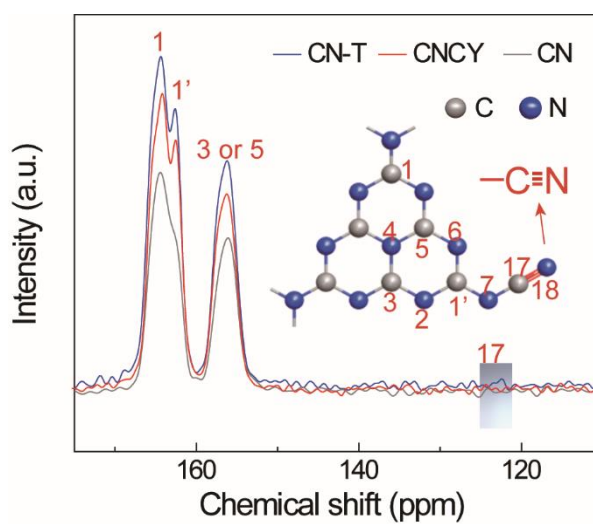
Figure S7. S 2p spectra of CN, CNCY and CN-T.

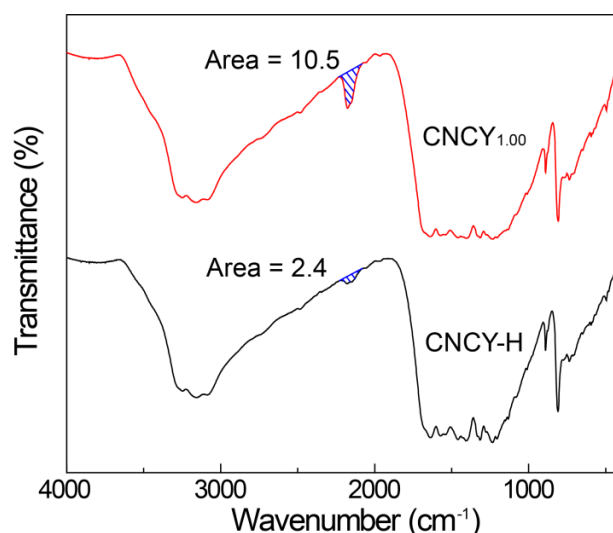**Figure S8.** Solid-state ^{13}C MAS NMR spectra of CN, CNCY and CN-T.

Figure S9. The FT–IR spectra of CNCY and CNCY–H.

As shown in Figure S9, after sample CNCY was refluxed in 3M sulphuric acid for 2 h, the cyano area which calculated by using the OMNIC software is decreased from 10.5 to 2.4. That indicates about 77.1% of the cyano group had been hydrolyzed to carboxylic acid. The titration results of carboxyl group in $CNCY_{1.00}$–H is 0.40 mmol/g (Table S5, entry 2), thus the total cyano content in $CNCY_{1.00}$ is about 0.52 mmol/g (0.4 / 0.771 = 0.52) and the mass percent is about 1.5 wt% [(0.52 mmol/g × 1 g × 26 g/mol)/1g × 100 wt% = 1.5 wt%]. The total cyano content in CN-T is about 0.62 mmol/g, then the mass percent is about 1.8 wt% [(0.62 mmol/g × 1 g × 26 g/mol)/1g × 100 wt% = 1.8 wt%]. The treatment and cyano group conversion methods of other samples in entries 3-10 were same to CNCY and CN-T. The detailed cyano group content of each sample was summarized in Table S5.
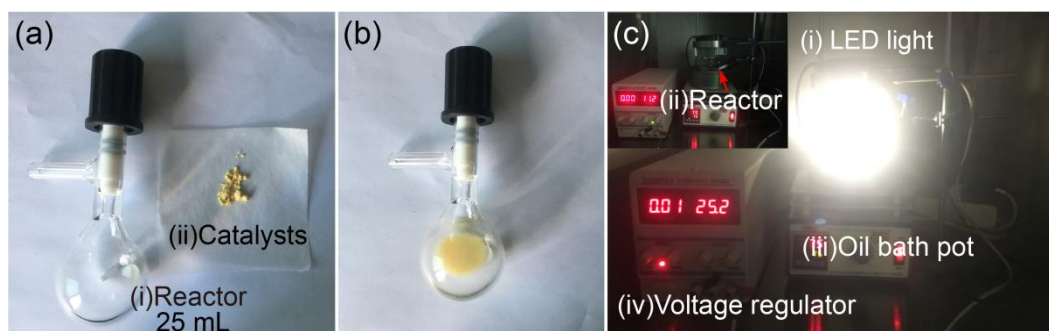
Figure S10. Images of the experimental setups for (a) reactor (b) with reactant and catalyst loaded and (c) photocatalytic oxidation reactions.
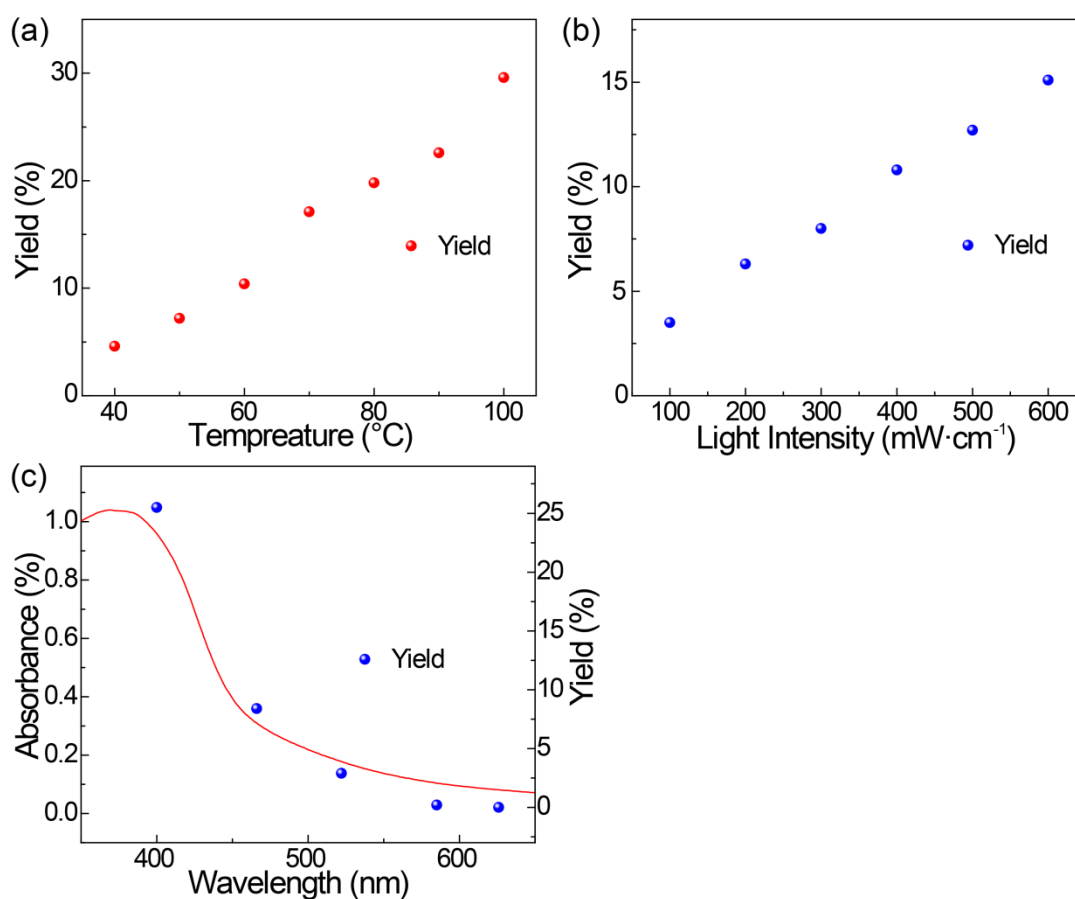

Figure S11. Influence of (a) temperature (b) light intensity and (c) wavelength (purple 400 nm, blue 459 nm, green 525 nm, yellow 580 nm, red 625 nm) on the epoxidation of styrene.

Reaction condition: 0.04 mmol of styrene, 2 mL of acetonitrile, 10 mg of the catalyst, 1 atm Air, white LED light, 4 h. (a) 400 mW/cm^2 irradiation, (b) 60 °C (c) 400 mW/cm^2 irradiation, 60 °C.
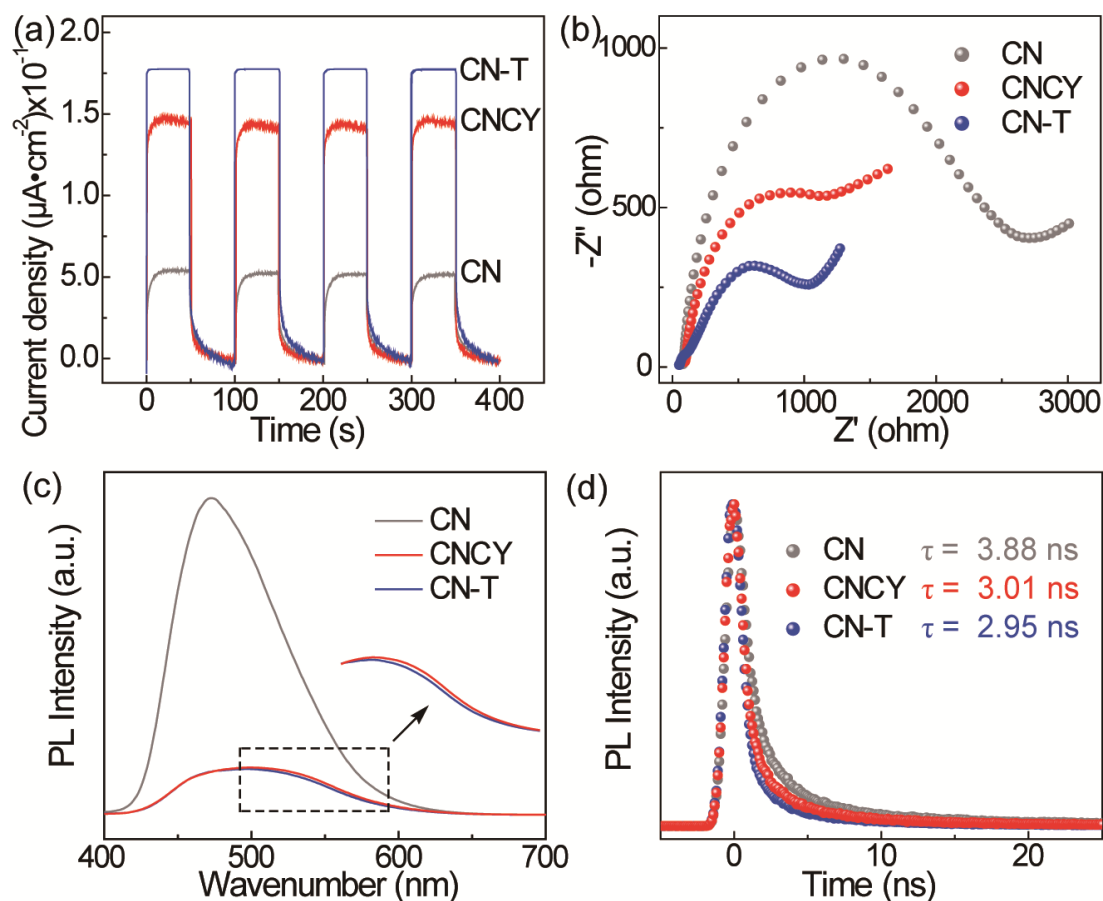
Figure S12. Optical, electronic properties and catalytic performance of varied carbon nitride catalysts. (a) Photocurrent response. (b) EIS Nyquist plots of CN, CNCY and CN-T. (c) Steady–state and (d) time–resolved photoluminescence decay spectra of CN, CNCY and CN-T at λ_{ex} = 365 nm.

The generation and separation efficiency of photogenerated carriers were measured by three classic methods: transient photocurrent, electrochemical impedance spectroscopy and photoluminescence.[12] The transient photocurrent of the samples was prompt by the on/off of intermittent visible-light irradiation (λ > 420 nm) in 0.2 M Na_2SO_4 aqueous solution. An obvious increase of photocurrent density was observed from CN to CNCY and CN-T (Figure S12a). The electrochemical impedance spectroscopy (EIS) in the dark was carried out. It can be seen that the arc radius decreases in the order of CN > CNCY > CN-T, indicating less resistance of charge

across the cyano modified sample film electrode interface (Figure S12b).[13] The steady–state photoluminescence (PL) and the time–resolved PL spectra were monitored under the excitation wavelength of 365 nm. For CN, the strong PL emission at 470 nm shows high charge carriers recombination efficiency. After cyano group modification, the intensity of this emission peak is weakened (Figure S12c). Time-resolved PL yield the mean radiative lifetimes of 3.88, 3.01 and 2.95 ns for CN, CNCY and CN-T, respectively (Figure S12d). The decreased singlet exciton lifetime clearly suggests enhanced singlet exciton dissociation and more effective separation of photogenerated electron–hole pairs in CN-T,[14] which is consistent with the result of photocurrent and EIS result. These results all indicate that the cyano group modification could improve the carrier generation and separation efficiency.[15]
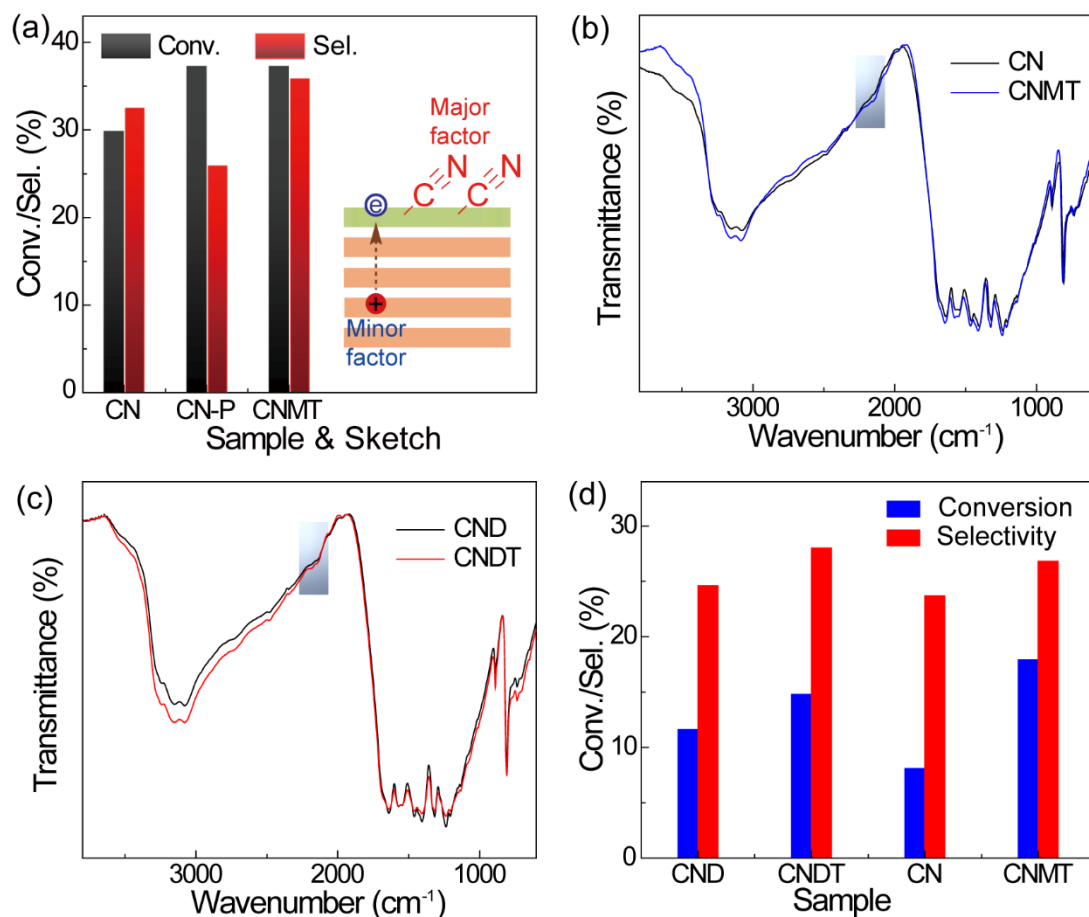
Figure S13. Catalytic performance comparison between CN, CN-P and CNMT for epoxidation of styrene. The inset diagram in Figure S13a is the sketch exhibited the major and minor factor which affect the performance of the catalyst. FT–IR spectra of (b) CN, CNMT and (c) CND, CNDT. (d) Catalytic performance comparison between CN, CNMT, CND and CNDT for epoxidation of styrene.

Reaction conditions: 0.04 mmol of styrene, 2 mL of acetonitrile, 15 mg of catalyst, 1 atm air, 400 mW/cm^2, white LED light irradiation, 60 °C, 4 h. Selectivity = Selectivity for styrene oxide.
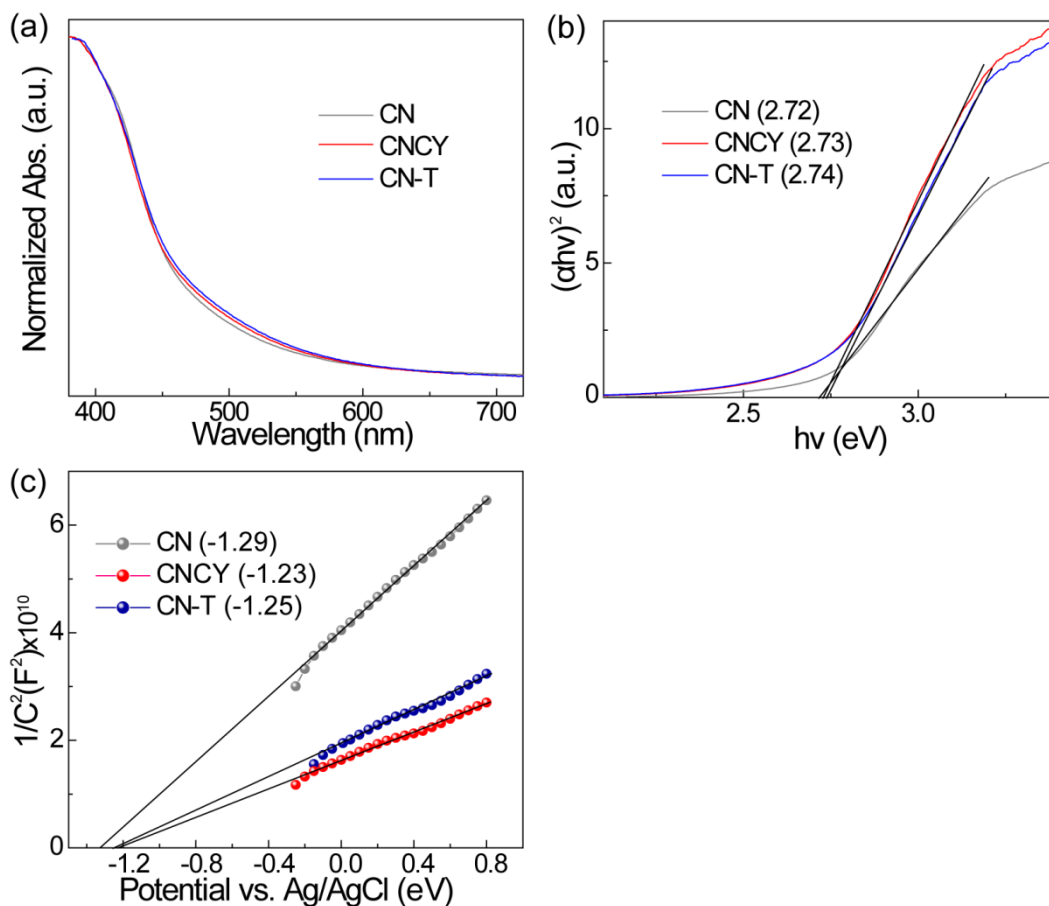
Figure S14. (a) UV–Vis patterns (b) band gap energy and (c) Mott–Schottky plots.

The band gap obtained from UV–Vis curves of CN, CNCY and CN-T were 2.72, 2.73 and 2.74 eV, respectively (Figure S14a and b). That indicates cyano group modifying caused a slightly enlarged band gap, which attributes to the quantum effect caused by formation thin layer structure.[16] However, this does not affect the utilization the energy of light. On account of sample CNCY and CN-T showed a tail absorption (Urbach tail) in the visible-light region (Figure S14a), which indicates that a midgap state is created by the cyano introduction.[12] Thus, the CNCY$_x$ samples can absorb more visible light, which will promote the solar light utilization efficiency. The Mott–Schottky curves showed in Figure S14c indicate a typical *n*-type plot for all samples. According to these plots, the flat band potentials of CN, CNCY, and CN-T were determined to be

at -1.29, -1.23 and -1.25 V *vs.* Ag/AgCl at pH = 6.6, which correspond to -0.76 V, -0.64 V and

-0.66 V *vs.* SHE at pH = 0, respectively (according to eq. s5 and eq. s6)

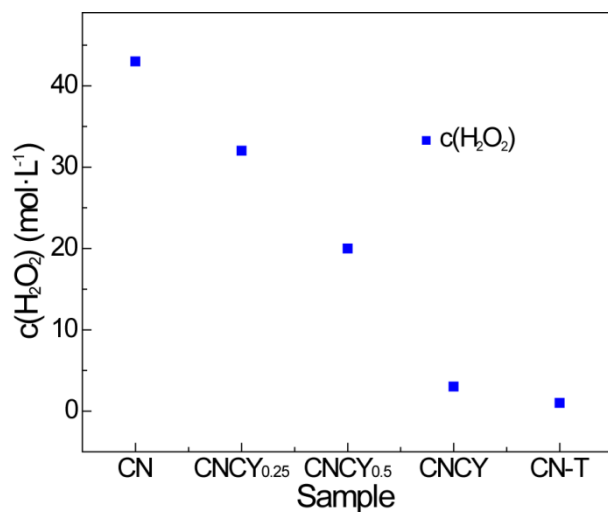**Figure S15.** (a) The yield of H_2O_2 as the function of various catalysts.
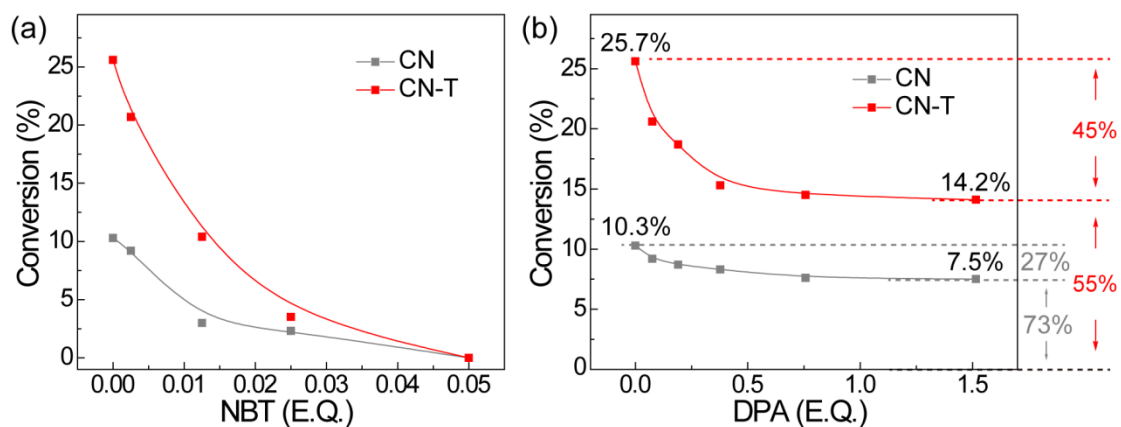

Figure S16. (a) Conversion and selectivity of styrene oxide as the function of nitroblue

tetrazolium amount (NBT) and (b) 9,10–Diphenylanthracene (DPA) amount.

Reaction conditions: 0.04 mmol of the styrene, 2 mL of the acetonitrile, 10 mg of the catalyst, 1

atm Air, 400 mW/cm^2 irradiation, white LED light, 60 °C, 4 h.
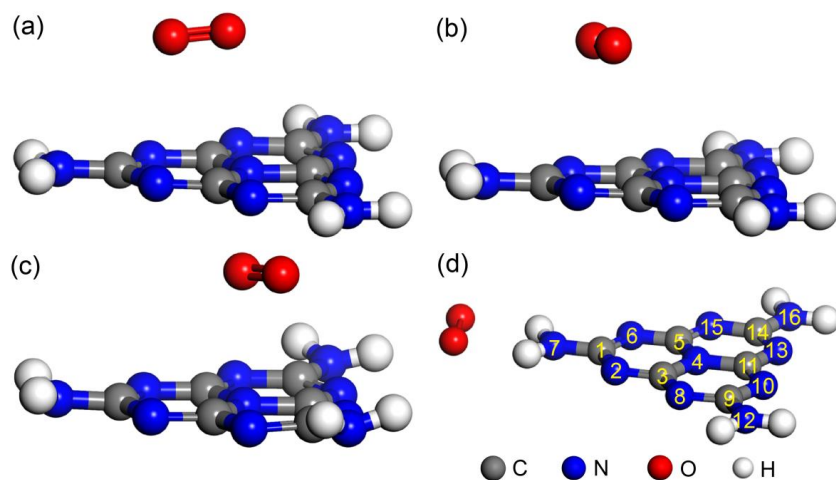
Figure S17. The optimized dioxygen adsorption mode on CN. The single-state O_2 initially located above the (a)N4-C1, (b) N6-C3, (c) N4-C11, and (d) N7-C1.

After the interaction of single-state O_2 with CN, the optimized configurations in Figure S17a is the most stable compared to the other adsorption configurations, in which the single-state O_2 is located above the N4-C1 site, the adsorption energy was summarized in Table S7.
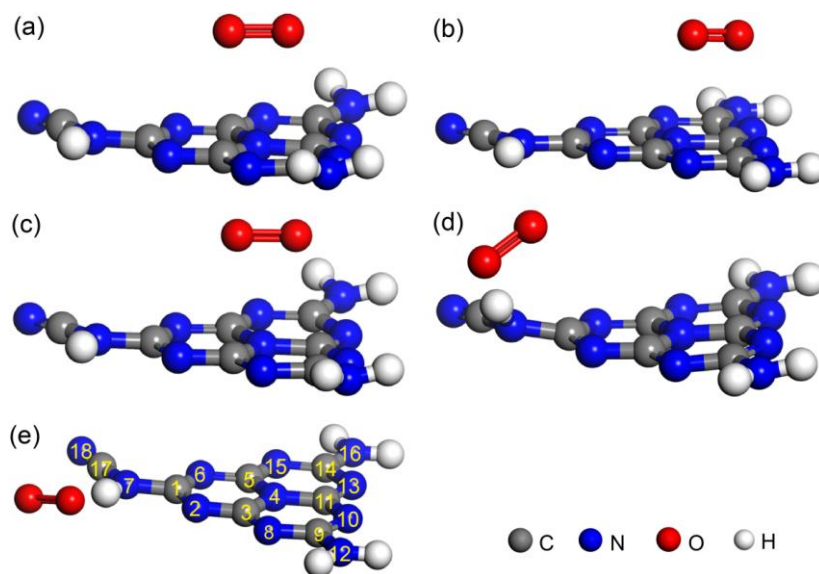
Figure S18. Other five types of the optimized dioxygen adsorption mode on cyano modified carbon nitride. The single-state O_2 initially located above the (a) N4-C1, (b) C3-N10, (c) N4-C11, (d) C17-N18 and (e) N7-H.
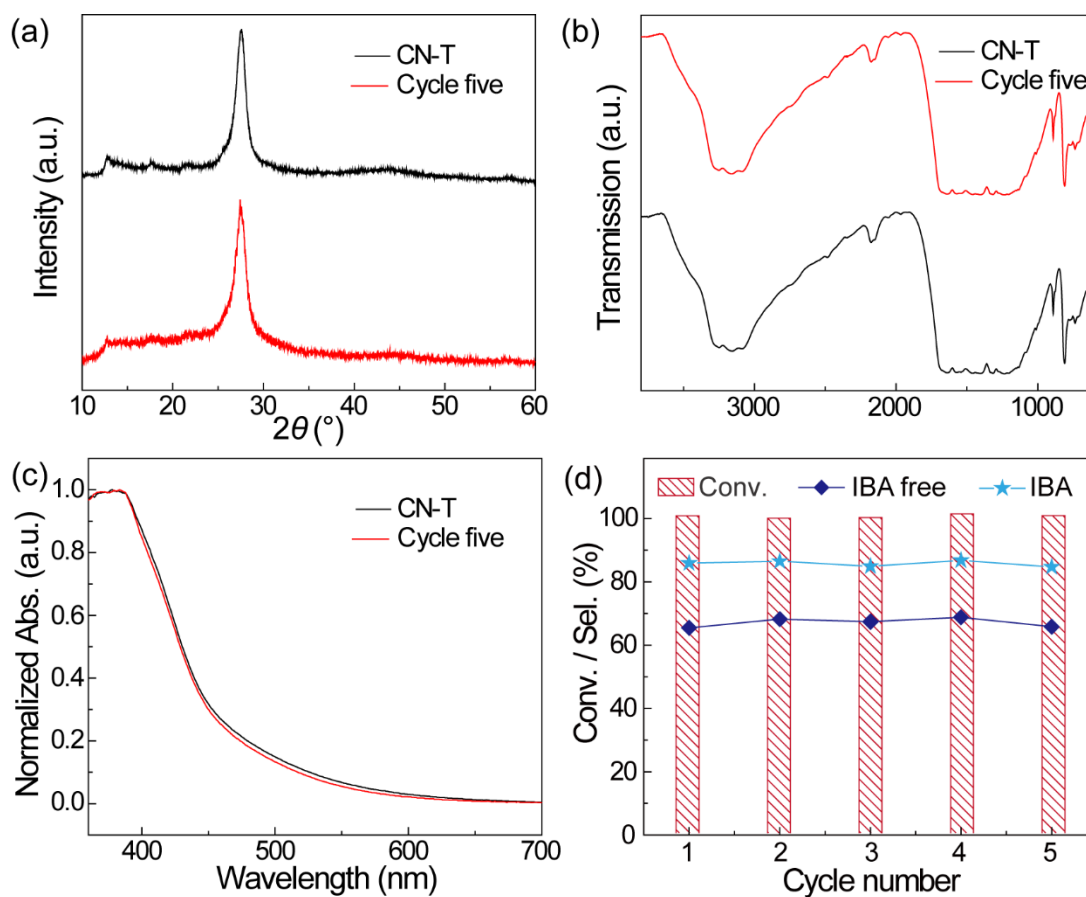
Figure S19. (a) XRD (b) FT–IR and (c) UV–Vis patterns of sample CN-T after being recycled five times. (d) Cycling performance of CN-T. Diamond: the epoxy products selectivity in the absence of isobutyraldehyde (IBA) as reducing agent. Star: the epoxy products selectivity in the presence of IBA.

Reaction conditions: 0.04 mmol of styrene, 2 mL of acetonitrile, 10 mg of catalyst, 1 atm air, white LED illumination (400 mW/cm^2), 60 °C, 24 h for isobutyraldehyde free and 2 h for isobutyraldehyde added system.

Table S1. Summary of the yield of styrene oxide in 15 literatures.

Entry	Samples	Conv. (%)	Sel.$_{epoxide}$ (%)	Yield$_{epoxide}$ (%)	Ref
1	Fe^{2+}–NaY	46.2	62.2	28.7	17
2	Fe_3O_4	38.0	56.5	21.5	17
3	Co^{2+}–X	44.2	60.0	26.5	18
4	$CoCl_2$	90.0	0	0	19
5	Co–Y–ZrO_2	61.0	80.0	48.8	20
6	Ga–Co–HMS–X	99.9	67.5	67.4	21
7	NHPI/Fe(BTC)	7.0	14.0	1.0	22
8	AuNC@N–C	96.8	40.4	39.1	23
9	La–MCM–48	54.5	98.8	53.8	24
10	N–OLC	88.4	46.0	40.7	25
11	OMCA–10	75.8	56.6	42.9	26
12	BaO/Ga_2O_3	49.3	58.0	28.6	27
13	VS–1(1)	70.0	44.0	30.8	28
14	$Au_{25}(SR)_{18}$	36.6	32.0	11.7	29
15	Ti(OiPr)$_4$/ligand	73.0	71.0	51.8	30
16	P450 enzymes	96.0	50.0	48.0	31

Table S2. Physicochemical properties of CN, CNCY and CN-T.

Sample	Pore volume (cm^3/g)	S_{BET} (m^2/g)
CN	0.12	14.2
CNCY	0.37	61.3
CN-T	0.45	65.6

Table S3. Distribution of element species obtained from the deconvolution of the N1s peaks by XPS.

Sample	Area / Proportion (%)		
	C-N=C	**N-(C)$_3$**	**C-N-H**
CN	80626.8 / 74.0%	24289.3 / 22.3%	4096.2 / 3.8%
CNCY	93936.4 / 74.2%	28330.6 / 22.4%	4303.8 / 3.4%
CN-T	76891.8 / 74.2%	23710.3 / 22.9%	3060.2 / 3.0%

The proportion of C-N-H component was calculated by dividing the peak area of C-N-H by the total area.

Table S4. Distribution of element species obtained from the deconvolution of the C1s peaks by XPS.

Sample	Area			$\mathbf{Area_{(C\text{-}NHx\ \&\ C\equiv N)}}$ / $\mathbf{Area_{(N\text{-}C=N)}}$
	C-C	**N-C=N**	**C-NH$_x$ & C≡N**	
CN	6259.6	45623.4	1406.2	0.03
CNCY	1165.5	47448.7	1423.5	0.03
CN-T	12187.6	43421.9	1302.7	0.03

The proportion of C-H$_x$ & C≡N component was calculated by dividing the peak area of C-H$_x$ & C≡N by the area of N-C=N.

Table S5. The content variation of cyano and carboxyl groups on the cyano modified samples.

Entry	Sample	Cyano group area	Conv.area (%)	Carboxyl (mmol/g)	Cyano group Estimated value (mmol/g)
1	CNCY	10.5	0	0	0
2	CNCY–H	2.4	77.1	0.40	0.52
3	$CNCY_{0.25}$	2.3	0	0	0
4	$CNCY_{0.25}$–H	0.56	75.6	0.08	0.11
5	$CNCY_{0.40}$	3.8	0	0	0
6	$CNCY_{0.40}$–H	0.72	81.1	0.15	0.19
7	$CNCY_{0.50}$	5.0	0	0	0
8	$CNCY_{0.50}$–H	1.07	78.6	0.20	0.25
9	$CNCY_{0.75}$	7.8	0	0	0
10	$CNCY_{0.75}$–H	1.61	79.3	0.31	0.39
11	CN-T	12.6	78.6	0.49	0.62
12	CN-T-H	2.7	0	0	0

Table S6. The catalytic and photoelectric performance of CN and CN–P.

Entry	Sample	Conv. (%)	Sel.styrene oxide (%)	Photocurrent density ($\mu A/cm^2$)	Electrochemical impedance (Ω)	Fluorescence lifetime (ns)
1	CN	31.9	33.6	0.051	4800	3.88
2	CN–P	37.5	25.4	0.062	3100	3.56

Reaction condition: 0.04 mmol of styrene, 2 mL of acetonitrile, 10 mg of the catalyst,1 atm Air, 60 °C, white LED light, 400 mW/cm² irradiation, 12 h.

The CN–P sample was prepared by heating melamine (10 g) and ammonium phosphate (0.25 g) mixture in a muffle furnace at 550 °C for 4 h.
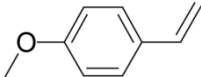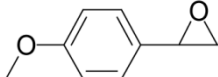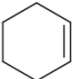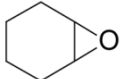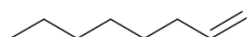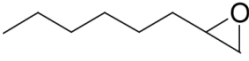
Table S7. The adsorption energy related Figure S16.

Entry	Initial site	Total energy (Ha)	Relative energy (kJ/mol)
1	N4-C1	-929.5073504	-39.1
2	N6-C3	-929.5009105	-22.2
3	N4-C11	-929.494547	-5.5
4	N7-C1	-929.4924522	0.0

Table S8. The adsorption energy related Figure S17.

Entry	Initial site	Total energy (Ha)	Relative energy (kJ/mol)
1	N7-C17	-1021.647935	-39.3
2	N7-N18	-1021.647874	-39.1
3	N4-C1	-1021.643873	-28.6
4	C3-N10	-1021.643673	-28.1
5	N4-C11	-1021.643933	-28.8
6	C17-N18	-1021.639660	-17.5
7	N7-H	-1021.632977	0.0

Table S9. Scope of the CN-T catalyzed epoxidation reaction of alkenes.

Entry	Substrates	Products	Conversion (%)	Selectivity (%)
1			99.6	65.8
2			99.6	54.5
3			99.9	99.9
4			13	60.1

Reaction conditions: 0.04 mmol of the alkenes, 2 mL of the acetonitrile, 10 mg of the catalyst, 1 atm Air, 400 mW/cm^2 irradiation, white LED light, 60 °C, 24 h.

Supplemental References

1.   Lau, V.W.H., Moudrakovski, I., Botari, T., et al. Rational Design of Carbon Nitride Photocatalysts by Identification of Cyanamide Defects as Catalytically Relevant Sites. *Nat. Commun.* **7**, 12165-12174 (2016). 10.1038/ncomms12165 https://www.nature.com/articles/ncomms12165#supplementary-information

2.   Niu, P., Qiao, M., Li, Y., et al. Distinctive Defects Engineering in Graphitic Carbon Nitride for Greatly Extended Visible Light Photocatalytic Hydrogen Evolution. *Nano Energy* **44**, 73-81 (2018). https://doi.org/10.1016/j.nanoen.2017.11.059

3.   Yuan, B., Chu, Z., Li, G., et al. Water-Soluble Ribbon-Like Graphitic Carbon Nitride (*g*-C$_3$N$_4$): Green Synthesis, Self-Assembly and Unique Optical Properties. *J. Mater. Chem. C* **2**, 8212-8215 (2014). 10.1039/C4TC01421A

4.   Yu, H., Shi, R., Zhao, Y., et al. Alkali-Assisted Synthesis of Nitrogen Deficient Graphitic Carbon Nitride with Tunable Band Structures for Efficient Visible-Light-Driven Hydrogen Evolution. *Adv. Mater.* **29**, 1605148-1605156 (2017). 10.1002/adma.201605148

5.   Liu, G., Zhao, G., Zhou, W., et al. In Situ Bond Modulation of Graphitic Carbon Nitride to Construct p–n Homojunctions for Enhanced Photocatalytic Hydrogen Production. *Adv. Funct. Mater.* **26**, 6822-6829 (2016). 10.1002/adfm.201602779

6.   Delley, B. An All-Electron Numerical-Method for Solving the Local Density Functional for Polyatomic-Molecules. *J Chem. Phys.* **92**, 508-517 (1990). 10.1063/1.458452

7.   Delley, B. From Molecules to Solids with the DMol^3 Approach. *J Chem. Phys.* **113**, 7756-7764 (2000). 10.1063/1.1316015

8.   Tian, D., Zhang, H. and Zhao, J. Structure and Structural Evolution of Agn (n=3–22) Clusters using a Genetic Algorithm and Density Functional Theory Method. *Solid State Commun.* **144**, 174-179 (2007). https://doi.org/10.1016/j.ssc.2007.05.020

9.   Perdew, J.P., Burke, K. and Ernzerhof, M. Generalized Gradient Approximation Made Simple. *Phys. Rev. Lett.* **77**, 3865-3868 (1996). 10.1103/PhysRevLett.77.3865

10. Hohenberg, P. and Kohn, W. Inhomogeneous Electron Gas. *Phys. Rev.* **136**, B864-B871 (1964). 10.1103/PhysRev.136.B864

11. Inada, Y. and Orita, H. Efficiency of Numerical Basis Sets for Predicting the Binding Energies of Hydrogen Bonded Complexes: Evidence of Small Basis Set Superposition Error Compared to Gaussian Basis Sets. *J. Comput. Chem.* **29**, 225-232 (2008). 10.1002/jcc.20782

12. Tan, H., Gu, X., Kong, P., et al. Cyano Group Modified Carbon Nitride with Enhanced Photoactivity for Selective Oxidation of Benzylamine. *Appl. Catal. B. Environ.* **242**, 67-75 (2019). https://doi.org/10.1016/j.apcatb.2018.09.084

13. Wang, J., Yang, Z., Yao, W., et al. Defects Modified in the Exfoliation of *g*-C$_3$N$_4$ Nanosheets Via a Self-Assembly Process for Improved Hydrogen Evolution Performance. *Appl. Catal. B. Environ.* **238**, 629-637 (2018). https://doi.org/10.1016/j.apcatb.2018.07.017

14. Ou, H., Chen, X., Lin, L., et al. Biomimetic Donor–Acceptor Motifs in Conjugated Polymers for Promoting Exciton Splitting and Charge Separation. *Angew. Chem. Int. Ed.* **57**, 8729-8733 (2018). 10.1002/anie.201803863

15.   Li, Y., Ouyang, S., Xu, H., et al. Constructing Solid–Gas-Interfacial Fenton Reaction over Alkalinized-C_3N_4 Photocatalyst to Achieve Apparent Quantum Yield of 49% at 420 nm. *J. Am. Chem. Soc.* **138**, 13289-13297 (2016). 10.1021/jacs.6b07272

16.   Xiao, Y., Tian, G., Li, W., et al. Molecule Self-Assembly Synthesis of Porous Few-Layer Carbon Nitride for Highly Efficient Photoredox Catalysis. *J. Am. Chem. Soc.* **141**, 2508-2515 (2019). 10.1021/jacs.8b12428

17.   Liang, J., Zhang, Q., Wu, H., et al. Iron-Based Heterogeneous Catalysts for Epoxidation of Alkenes using Molecular Oxygen. *Catal. Commun.* **5**, 665-669 (2004). https://doi.org/10.1016/j.catcom.2004.08.010

18.   Tang, Q., Wang, Y., Liang, J., et al. Co^{2+}-Exchanged Faujasite Zeolites as Efficient Heterogeneous Catalysts for Epoxidation of Styrene with Molecular Oxygen. *Chem. Commun.*, 440-441 (2004). 10.1039/B314864E

19.   Lin, Y.H., Williams, I.D. and Li, P. Selective Oxidation of Styrenes under Oxygen Catalyzed by Cobalt Chloride. *Appl Catal A-Gen* **150**, 221-229 (1997). https://doi.org/10.1016/S0926-860X(96)00187-1

20.   Tyagi, B., Shaik, B. and Bajaj, H.C. Epoxidation of Styrene with Molecular O_2 over Sulfated $Y–ZrO_2$ Based Solid Catalysts. *Appl Catal A-Gen* **383**, 161-168 (2010). https://doi.org/10.1016/j.apcata.2010.05.038

21.   Rahman, S., Santra, C., Kumar, R., et al. Highly Active Ga Promoted Co-HMS-X Catalyst Towards Styrene Epoxidation Reaction using Molecular O_2. *Appl. Catal. A: Gen.* **482**, 61-68 (2014). https://doi.org/10.1016/j.apcata.2014.05.024

22.   Dhakshinamoorthy, A., Alvaro, M. and Garcia, H. Aerobic Oxidation of Styrenes Catalyzed by an Iron Metal Organic Framework. *ACS Catal.* **1**, 836-840 (2011). 10.1021/cs200128t

23.   Liu, B., Wang, P., Lopes, A., et al. Au–Carbon Electronic Interaction Mediated Selective Oxidation of Styrene. *ACS Catal.* **7**, 3483-3488 (2017). 10.1021/acscatal.7b01048

24.   Zhan, W., Guo, Y., Wang, Y., et al. Study of Higher Selectivity to Styrene Oxide in the Epoxidation of Styrene with Hydrogen Peroxide over La-Doped MCM-48 Catalyst. *J. Phys. Chem. C* **113**, 7181-7185 (2009). 10.1021/jp8101095

25.   Lin, Y., Pan, X., Qi, W., et al. Nitrogen-Doped Onion-Like Carbon: A Novel and Efficient Metal-Free Catalyst for Epoxidation Reaction. *J. Mater. Chem. A* **2**, 12475-12483 (2014). 10.1039/C4TA01611D

26.   Pan, D., Xu, Q., Dong, Z., et al. Facile Synthesis of Highly Ordered Mesoporous Cobalt–Alumina Catalysts and Their Application in Liquid Phase Selective Oxidation of Styrene. *RSC Adv.* **5**, 98377-98390 (2015). 10.1039/C5RA20531J

27.   Choudhary, V.R., Jha, R. and Jana, P. Epoxidation of Styrene by TBHP to Styrene Oxide using Barium Oxide as a Highly Active/Selective and Reusable Solid Catalyst. *Green Chem.* **8**, 689-690 (2006). 10.1039/B604937K

28.   Singh, B. and Sinha, A.K. Synthesis of Hierarchical Mesoporous Vanadium Silicate-1 Zeolite Catalysts for Styrene Epoxidation with Organic Hydroperoxide. *J. Mater. Chem. A* **2**, 1930-1939 (2014). 10.1039/C3TA13451B

29.   Zhu, Y., Qian, H., Zhu, M. and Jin, R. Thiolate-Protected Aun Nanoclusters as Catalysts for Selective Oxidation and Hydrogenation Processes. *Adv. Mater.* **22**, 1915-1920 (2010). 10.1002/adma.200903934

30. Matsumoto, K., Oguma, T. and Katsuki, T. Highly Enantioselective Epoxidation of Styrenes Catalyzed by Proline-Derived C1-Symmetric Titanium(Salan) Complexes. *Angew. Chem. Int. Ed.* **48**, 7432-7435 (2009). 10.1002/anie.200903567

31. Wang, L., Wei, S., Pan, X., et al. Enhanced Turnover for the P450 119 Peroxygenase-Catalyzed Asymmetric Epoxidation of Styrenes by Random Mutagenesis. *Chem.Eur.J.* **24**, 2741-2749 (2018). 10.1002/chem.201705460